

Two Candidate Obscured Tidal Disruption Events Coincident with High-energy Neutrinos

NING JIANG ^{1,2} ZIYING ZHOU ^{1,2} JIAZHENG ZHU ^{1,2} YIBO WANG ^{1,2} AND TINGGUI WANG ^{1,2}

¹CAS Key laboratory for Research in Galaxies and Cosmology, Department of Astronomy, University of Science and Technology of China, Hefei, 230026, China; jnac@ustc.edu.cn

²School of Astronomy and Space Sciences, University of Science and Technology of China, Hefei, 230026, China

ABSTRACT

Recently, three optical tidal disruption event (TDE) candidates discovered by the Zwicky Transient Facility (ZTF) have been suggested to be coincident with high-energy neutrinos. They all exhibit unusually strong dust infrared (IR) echoes, with their peak times matching the neutrino arrival time even better than the optical peaks. We hereby report on two new TDE candidates that are spatially and temporally coincident with neutrinos by matching our sample of mid-infrared outbursts in nearby galaxies (MIRONG) with Gold alerts of IceCube high-energy neutrino events up to June 2022. The two candidates show negligible optical variability according to their ZTF light curves and can therefore be classified as part of the growing population of obscured TDE candidates. The chance probability of finding two such candidates about $\sim 3\%$ by redistributing the MIRONG sources randomly in the SDSS footprint, which will be as low as $\sim 0.1\%$ (or $\sim 0.2\%$) if we limit to sources with increased fluxes (or variability amplitudes) comparable with the matched two sources. Our findings further support the potential connection between high-energy neutrinos and TDEs in dusty environments by increasing the total number of neutrino-associated TDE and TDE candidates to five, although the underlying physics remains poorly understood.

Keywords: Tidal disruption (1696) — Neutrino astronomy (1100) — Supermassive black holes (1663) — High energy astrophysics (739) — Time domain astronomy (2109)

1. INTRODUCTION

Since the detection of TeV-PeV cosmic neutrinos by the IceCube neutrino observatory in 2013 (IceCube Collaboration 2013), the number of high-energy neutrinos has steadily increased. However, their astrophysical origin remains a hotly debated topic and is one of the most cutting-edge areas of research in multi-messenger astronomy. Despite the increasing number of high-energy neutrinos detected, no significant cluster in space or time has been found while there is a tentative correlation with the nearby Seyfert galaxy NGC 1068 at the 4.2σ level (Aartsen et al. 2020; IceCube Collaboration et al. 2022). Therefore, identifying electromagnetic counterparts of high-energy neutrinos remains extremely challenging.

A complementary approach is to directly search for electromagnetic counterparts to individual high-energy neutrinos that have a high probability of being of astrophysical origin. However, only three candidates of electromagnetic counter-

parts have been identified at the $\sim 3\sigma$ level to date based on both spatial and temporal coincidence. The first ever identification was the flaring blazar TXS 0506+056 (IceCube Collaboration et al. 2018) with neutrino alert IC170922A during a period of electromagnetic flaring in 2017. The latter two were identified as a tidal disruption event (TDE, Gezari 2021) and a TDE candidate, respectively. TDEs occur when an unlucky star wanders into the tidal sphere of a SMBH and gets ripped apart by the tidal force. Part of the disrupted stellar debris is accreted by the SMBH and produces an electromagnetic flare on timescales of months to years (Rees 1988). The discovery speed of TDEs has accelerated with the aid of modern optical time-domain surveys, particularly the Zwicky Transient Facility (ZTF), which has boosted the discovery rate from $\lesssim 2/\text{yr}$ per year to $> 10/\text{yr}$ (van Velzen et al. 2021a; Yao et al. 2023). Both objects, AT2019dsg and AT2019fdr, were initially discovered by ZTF, and their optical luminosity peaks occurred 150-300 days before the arrival time of the corresponding IceCube neutrino events, that is IC191001A (Stein et al. 2021, cf. Liao et al. 2022) and IC200530A (Reusch et al. 2022, cf. Pitik et al. 2022), respectively. AT2019dsg is a bonafide TDE and its property has been detailedly analyzed by works on ZTF TDE sam-

ple (van Velzen et al. 2021a; Hammerstein et al. 2023; Yao et al. 2023). In contrast, the TDE identification of AT2019fdr is rather uncertain as the flare happened in a known AGN, the origin of which is complicated by the existence of accretion disk (e.g., Graham et al. 2017; Trakhtenbrot et al. 2019; Frederick et al. 2021). The long-lived non-thermal emission detected in AT2019dsg (Stein et al. 2021; Cendes et al. 2021) indicates that the mildly relativistic outflows may be an ideal site for neutrino production. Both of the two neutrino emitters show unusually strong infrared (IR) echoes, which is the reprocessed emission of high-energy photons by the dust in the vicinity of the SMBHs (Jiang et al. 2016; van Velzen et al. 2016). Moreover, it is interesting to note that the arrival time of the neutrinos matches the peak time of the IR emission even better than the peak time of the optical emission.

Actually, most optical TDEs show very weak IR echoes, suggesting a dust-poor subparsec environment (Jiang et al. 2021b). The unusual properties of the neutrino-associated TDEs (or candidates) motivated a systematic search for similar nuclear transients with prominent IR echoes, and a third similar object AT2019aal, occurring in another known AGN, was found as the counterpart of IC191119A (van Velzen et al. 2021b). Moreover, they obtained a correlation at the 3.6σ confidence level between such flares and high-energy neutrino alerts. However, it should be noted that their search primarily started with the selection of optical flares in galactic nuclei with ZTF light curves, and as a result, all of these events are optically bright and presumably dust-unobscured. Nevertheless, an independent systematic search for mid-IR outbursts in nearby galaxies (MIRONG) suggests that a large fraction of nuclear transients might be optically weak (Jiang et al. 2021a). Therefore, if high-energy neutrinos are indeed connected with nuclear transients with strong IR echoes, as claimed by van Velzen et al. (2021b), the most efficient search for their counterparts should rely on the IR-selected sample, which is dominated by transient accretions onto SMBHs in dusty environments (Jiang et al. 2021a; Wang et al. 2022a), including unambiguous TDEs (Wang et al. 2022b). Most importantly, such TDEs can only be identified by IR echoes or radio emission if they are severely dust-obscured (e.g., Mattila et al. 2018; Kool et al. 2020; Panagiotou et al. 2023).

In this letter, we report the discovery of two obscured TDE candidates in the MIRONG sample that coincide spatially and temporally with high-energy neutrinos. We assume a cosmology with $H_0 = 70 \text{ km s}^{-1} \text{ Mpc}^{-1}$, $\Omega_m = 0.3$, and $\Omega_\Lambda = 0.7$.

2. DATA

2.1. The Neutrino Events

The IceCube Neutrino Observatory has detected high-energy astrophysical neutrinos that are statistically signifi-

cant above the atmospheric background. Since 2016, real-time alerts have been issued to the multi-messenger observational community for single high-energy ($>100 \text{ TeV}$) events via platforms such as the Global Cycling Network (GCN)¹. These alerts focus on track-like neutrino candidates, which offer more accurate angular localizations than cascade events. All alerts since June 2019 are assigned a signalness value and marked as gold or bronze depending on the chance of astrophysical origin, i.e., larger than 50% and 30%, respectively. The 90% containment error radius ("ERROR90") of these events ranges from 0.4 to 6.2 degrees, with an average of 1.5 degrees, not including systematic error. Note that for most neutrinos, a more accurate position is provided after the original one. These updated positions and their corresponding 90% containment errors are adopted in our analysis². The occurrence rate is expected to be one per month. For our analysis, we use the list of gold alerts between June 2019 and June 2022. Moreover, we only consider neutrinos with "ERROR90" less than 200 arcmin, which finally includes a total of 33 events (see Figure 1 and a full list in Table A1 in the Appendix).

2.2. The parent MIRONG Sample

The objects we match with high-energy neutrinos are from the MIRONG sample, which was constructed by a systematic search of low-redshift ($z < 0.35$) Sloan Digital Sky Survey (SDSS) spectroscopic galaxies with recent mid-IR flares. These objects were identified using archival data from the Wide-field Infrared Survey Explorer (WISE, Wright et al. 2010) and its new mission, the Near-Earth Object WISE (NEOWISE, Mainzer et al. 2014). The original sample, using data up to the end of 2018, resulted in a total of 137 objects with a brightening amplitude of 0.5 mag in at least one band with respect to their quiescent phases (Jiang et al. 2021a). In the current work, we extend the same search to the data as of the end of 2022, which is the most recent public NEOWISE dataset. The new MIRONG sample contains 269 objects, and its general properties remain the same as reported in Jiang et al. (2021a).

3. ANALYSIS AND RESULTS

3.1. Cross-match

The IR light curves for each object have been continuously sampled every six months in the WISE W1 ($3.4\mu\text{m}$) and W2 ($4.6\mu\text{m}$) bands since 2014. In order to temporally crossmatch

¹ https://gcn.gsfc.nasa.gov/amon_icecube_gold_bronze_events.html

² We also note that there is a recent paper (Abbasi et al. 2023) which has provided updated 90% containment for neutrinos between 2011 and 2020. However, we are mostly interested in the neutrinos between 2019 and 2022 since they are well overlapped with the ZTF survey timeline, which can offer crucial information on their optical emission and thus help diagnose their nature.

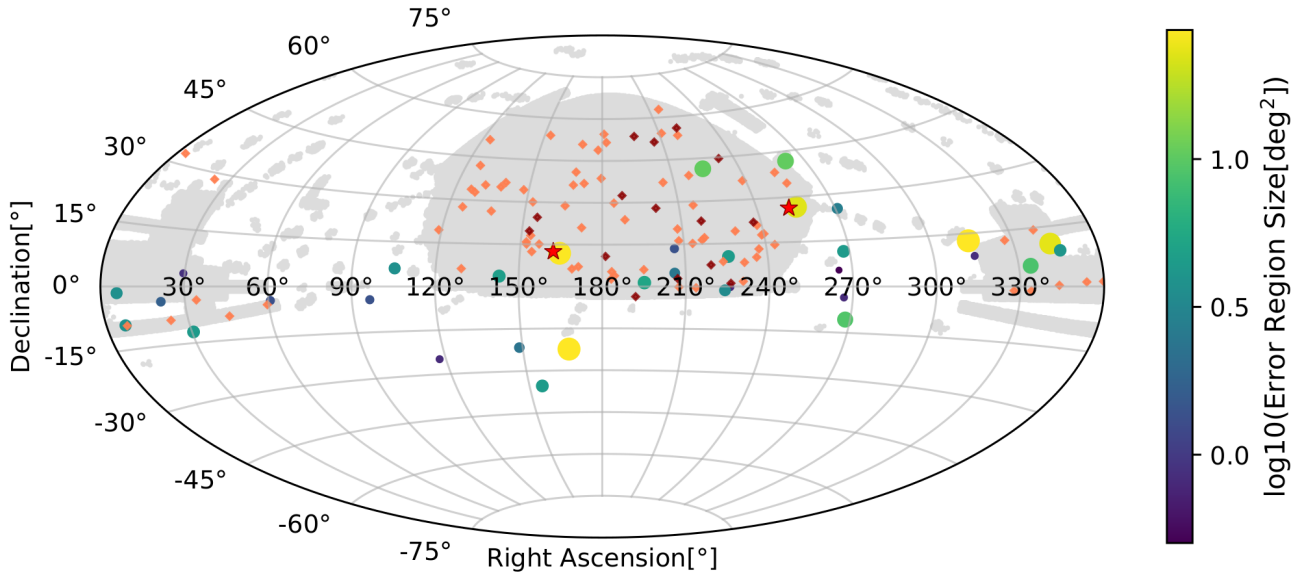


Figure 1. Sky map of observed high-energy neutrino event (Gold alerts) positions and their corresponding error region sizes, which are indicated by a colorbar on the right. The footprint of SDSS, from which our MIRONG sample is selected, is overplotted in grey overlay. The objects in our MIRONG sample with IR peaks at the same period are denoted as red diamonds and those with $W2 \leq 12.60$ are marked as dark red. The two sources that coincide with neutrinos are highlighted as red five-point stars. The clustering effect of the events around the equator region is due to the detector's high sensitivity in this area.

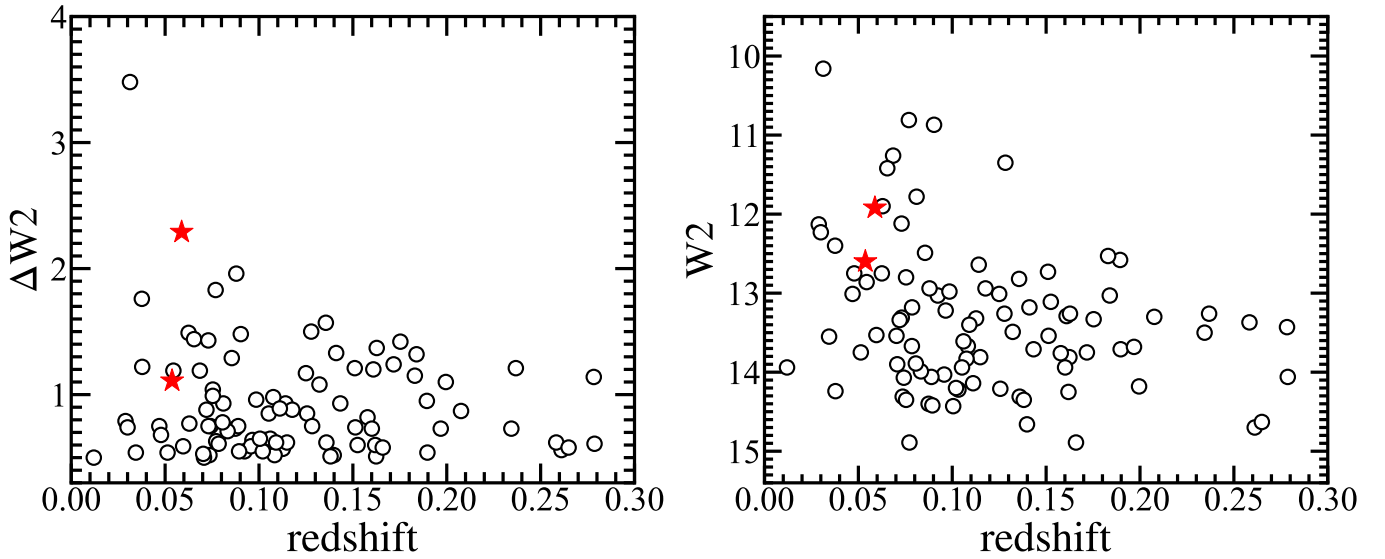


Figure 2. Left: the $W2$ variability amplitude ($\Delta W2$) vs. redshift distribution of the MIRONG sources used to match with neutrinos. Right: the $W2$ magnitude vs. redshift distribution. The two sources coincident with neutrinos are highlighted by red five-point stars.

potential sources with neutrinos, we only select those that exhibit peaks between June 2019 and June 2022, coinciding with the neutrino time range. The sources that are still in the rising stages as of the latest epoch (after June 2022) have been excluded. This process results in a total of 94 sources, which is listed in Table A2 in the Appendix. For each IceCube high-energy neutrino, there are its arrival time, NoticeType ("GOLD" or "BRONZE"), location (R.A., Decl.), energy, and signalness. Two location uncertainties, one with 90% ("ERROR90") and the other with 50% ("ERROR50") containment, are assigned. We only considered gold events and used the "ERROR90" location uncertainty as the matching radius. Furthermore, we define a temporal match by requiring that the time interval between the IR brightest epoch and the neutrino arrival is less than half a year, which is the WISE visit cadence.

Following above procedures, two outbursts in the MIRONG sample show both spatial and temporal coincidences with gold neutrinos. They are SDSSJ104832.79+122857.2 (hereafter SDSSJ1048+1228) and SDSSJ164938.77+262515.3 (SDSSJ1649+2625), matching with IceCube-200109A and IceCube-200530A, respectively (see their information in Table 1). Specifically, the MIR outburst in SDSSJ1048+1228 peaks on 2020 May 8 (MJD=58977) in WISE W2 band, which is four months ahead of IceCube-200109A while IceCube-200530A arrives about 2 months earlier than the IR peak time of SDSSJ1649+2625 on 2020 August 7 (MJD=59068). Spatially, the two neutrinos are 159 and 143 arcmins away from the two galaxies, yet they are consistent with each other within the 90% location uncertainties.

3.2. Probability by chance

We then attempt to calculate the probability of finding two such coincident events by chance. First, we perform a simple estimation following the method used in Stein et al. (2021). The area of the SDSS footprint and the total 90% containment area of the neutrinos in the SDSS footprint are 9376 deg² and 127.8 deg², respectively. There are 94 MIRONG sources peaked between June 2019 and June 2022, thus their number density is $94/9376/3 = 3.3 \times 10^{-3}/\text{deg}^2/\text{yr}$. Since we match the MIRONG sources with neutrinos by requesting their intervals are less than half year, the matching time window is thus 1 yr. The expectation value for the number of random matches is thus $3.3 \times 10^{-3} \times 127.8 = 0.427$, and then the probability of observing two or more matches is 0.069 based on Poisson statistics.

It is worthwhile to note that SDSSJ1048+1228 and SDSSJ1649+2625 belong to the lower-redshift (top 12%), larger amplitude (top 28%), and more apparently luminous (top 18%) subclass among the all sources (see Figure 2), indicating that the neutrino emission is likely related to a spe-

Table 1. Information of the matched MIR outbursts and neutrinos.

	SDSSJ1048+1228	SDSSJ1649+2625
redshift	0.0537	0.0588
BPT Type	LINER	Composite
Host Stellar mass ($\log M_*$)	10.86	9.13
$\log M_{\text{BH}}^a$	7.86	6.49
IR peak time	2020/05/08	2020/08/07
$\Delta W1/\Delta W2$	0.59/1.11	1.41/2.29
W1/W2 (peakmagnitude) ^b	13.65/12.60	13.09/11.92
IR peak luminosity	42.84	43.20
IR energy	50.72	51.02
Neutrino	IceCube-200109A	IceCube-200530A
NoticeType	GOLD	GOLD
Arrival Date	2020/01/09	2020/05/30
ERROR90	174.60	160.19
Energy	375.23	82.186

NOTE—

^a The mass of SMBH is estimated from $M_{\text{BH}} - \sigma_*$ relation following that in Jiang et al. (2021a).

^b The magnitude is for the emission with the quiescent-state flux subtracted.

cial population of MIRONG objects. One simple assumption is that the neutrino count is proportional to the observed MIR flux and thus the neutrino counterparts favour brighter MIR sources. If we restrict the sources to those with an increased flux comparable with the matched two, i.e. $W2 < 12.60$, the number of sources decreases from 94 to 17. As a result, the corresponding chance probability of finding two matches is calculated to be 0.0028. The other scenario is that the neutrinos are correlated with the IR variability amplitudes, as explored in the analysis conducted by van Velzen et al. (2021b). By limiting the MIRONG sources to those with variability amplitudes similar to the matched two, i.e. $\Delta W2 > 1$, the number of sources becomes 30 and the chance probability is then 0.0085.

We also try to estimate the probability by simulations. It should be noted that the flux limits of IceCube show a strong dependence on decl. (Aartsen et al. 2020). To account for this effect, we perform Monte Carlo simulations by redistributing the 33 gold neutrinos across sky taking into account the declinational dependence while with their distribution in right ascension entirely random. Specifically, the declination was redistributed according to the actual probability distribution

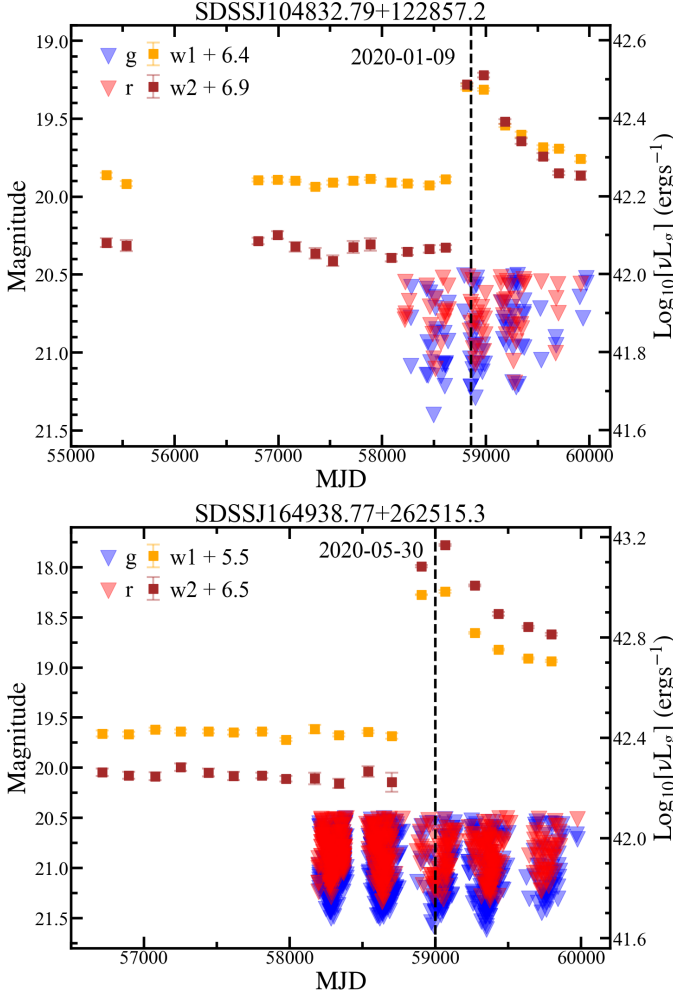


Figure 3. The MIR and optical light curves of SDSSJ1048+1228 and SDSSJ1649+2625. The NEOWISE photometry in W1 ($3.4\mu\text{m}$) and W2 ($4.6\mu\text{m}$) band are shown as orange and brown squares while the blue and red triangles represent the 3σ upper limits of ZTF forced difference photometry in g and r bands. The vertical dashed lines mark the arrival time of matched high-energy neutrinos IceCube-200109A and IceCube-200530A.

³. Furthermore, we did not alter the arrival time of neutrinos in our simulations since the timing of neutrino arrivals is random and not expected to have a significant impact on our results. We then match them spatially and temporarily with the MIRONG sources as described in §3.1. The experiment is repeated 30,000 times. The resulting probability of finding at least two matches is 0.0296 for 94 sources, which decreases to 0.0013 for 17 sources ($W2 < 12.6$) and decreases from 0.0049 for 30 sources ($\Delta W2 > 1$).

³ see Figure 3 in https://gcn.gsfc.nasa.gov/doc/IceCube_High_Energy_Neutrino_Track_Alerts_v2.pdf. We did not employ a parametric function to model the distribution. Instead, we simply assumed that the possibility within each histogram is evenly distributed.

Another alternative simulation involves shuffling the MIRONG sources while keeping the neutrinos fixed. This approach could be more reliable due to a relatively constant source density within the SDSS footprint, while the sky and temporal sensitivities of IceCube are challenging to quantify accurately. Therefore, we randomly redistributed the MIRONG sources within the SDSS footprint and subsequently matched them with neutrinos. The resulting chance probabilities of finding at least two matches are 0.025 and 0.0009 in the case without and with the requirement of $W2 < 12.6$, respectively, which are slightly lower than the case of shuffling neutrinos. Additionally, the probability is reduced to 0.0023 for the 30 sources with $\Delta W2 > 1$.

3.3. The Two Matched Sources as Obscured TDE candidates

The two MIR outbursts potentially associated with high-energy neutrinos lack detectable optical counterparts in public surveys such as ZTF (Masci et al. 2019, see Figure 3). In fact, as noted by Jiang et al. (2021a), the majority of the outbursts in the MIRONG sample have not been previously reported by any other surveys. This indicates that their optical emissions are either obscured or intrinsically weak.

Following the measurements performed on the entire MIRONG sample (Jiang et al. 2021a), we have fitted the MIR emission of SDSSJ1048+1228 and SDSSJ1649+2625 with blackbody model and found a peak luminosity of $10^{42.94}$ and $10^{43.29}$ erg s^{-1} , respectively. Such high IR luminosities almost exclude the supernova scenario and suggest that they are instead due to dust echoes of transient accretions onto SMBHs (Jiang et al. 2019, 2021a). Additionally, the integrated energies radiated in IR of the two sources are $10^{50.72}$ and $10^{51.02}$ erg as of the end of 2022, which are already comparable to the most energetic supernova (e.g., SN2016aps, Nicholl et al. 2020), but are rather typical for transient accretions such as TDEs (van Velzen et al. 2021c). Furthermore, both galaxies exhibit little or weak AGN activities according to their pre-outburst SDSS spectra (Figure 4), and have been classified as a LINER and a composite galaxy in the Baldwin-Phillips-Terlevich (BPT) diagram (Baldwin et al. 1981), respectively. It is worth noting that their MIR light curves show subtle variability (see Figure 3), This is particularly evident in the case of SDSSJ1048+1228, which suggests the possible presence of weak AGNs. Frederick et al. (2021) have recently reported the discovery a new class of changing-look LINERs, which pose a challenge in distinguishing them from TDEs for LINER galaxies. We conducted spectroscopic follow-up observations with the Double spectrograph (DBSP) mounted on the Hale 200 inch telescope (Oke & Gunn 1982) at Palomar observatory for SDSSJ1649+2625 on 2021 June 18 and with YFOSC of the LiJiang 2.4m telescope (Fan et al. 2015; Wang et al. 2019) at Yunnan obser-

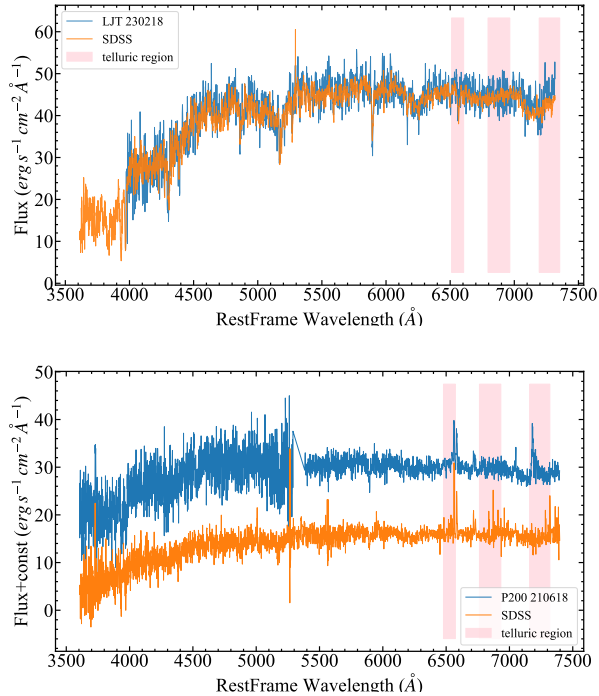


Figure 4. The optical spectra of SDSSJ1048+1228 and SDSSJ1649+2625. The archival SDSS spectrum are shown in orange while the new spectra taken after the outburst is shown in blue. No obvious spectral evolution is found for both objects.

vatories for SDSSJ1048+1228 on 2023 February 18. However, no obvious spectral evolution, i.e., emerging characteristic emission lines as seen in some of the MIRONG objects (Wang et al. 2022a), was found for both (see Figure 4). Therefore, we conclude that the two neutrino-matched MIR outbursts are highly consistent with the obscured counterparts of transient accretion onto SMBHs, such as TDEs or changing-look LINERs.

4. SUMMARY AND DISCUSSION

As a rare type of nuclear transient, TDEs have been regularly discovered by optical surveys and found being a possible production site of high-energy neutrinos over past few years. Interestingly, the initial two claimed sources, one robust TDE AT2019dsg and the other TDE candidate AT2019fdr, were both accompanied by bright IR echoes in stark contrast to normal optical TDEs. This indicates that the dust in the vicinity of SMBHs, which is assumed to be responsible for the reprocessed IR emission, could be a crucial factor in producing high-energy neutrinos. The unexpected neutrino-dust link then led to the identification of a third similar candidate, AT2019aalc. Moreover, the neutrino arrivals show great consistency with IR peaks, while they are hundreds of days delayed relative to the optical peak. The intriguing correlation between high-energy neu-

trinos and TDEs in dusty environments has motivated us to perform a new spatial and temporal cross-match of our own MIRONG sample, which is mainly caused by transient accretion onto SMBHs, with known gold alerts of high-energy neutrino events up to the end of 2022. This cross-match has resulted in the discovery of two new candidates, SDSSJ1048+1228 and SDSSJ1649+225. Despite exhibiting huge MIR flares, these candidates show non-detection in ZTF light curves and can be reasonably categorized as obscured TDE candidates. The probability of finding two such candidates by chance is about 3% based on our Monte Carlo simulations by shuffling the MIRONG sources in the SDSS footprint. The chance probability is much lower, that is about 0.1% ($\sim 3\sigma$), if we only consider sources with a increased flux comparable with the matched two ($W2 < 12.6$). Alternatively, if we restrict sources to those with a similar variability amplitude ($\Delta W2 > 1$), the chance probability is slightly larger, that is 0.2%.

One may wonder whether there are more matches if taking into consideration of bronze neutrinos. We have repeated the cross-match procedure and discovered two more matches: SDSSJ104832.79+122857.2 with IceCube-200620A and SDSSJ141249.70+151254.7 with IceCube-220205A. It is worth noting that SDSSJ104832.79+122857.2 coincides with both a gold neutrino and a bronze neutrino, indicating the possibility of it being a repeating neutrino emitter as the two neutrinos are separated by a five-month interval. In addition, the new source SDSSJ141249.70+151254.7 at $z = 0.1411$ shows a large variability amplitude ($\Delta W2 = 1.33$) yet with a lower increased flux ($W2 = 13.18$) due to a higher redshift in comparison with the formal two matched sources. The chance probability of matching at least four neutrinos with the 30 $\Delta W2 > 1$ sources keeps as low as $\sim 0.1\%$. In the future, we plan to employ a more advanced likelihood-based analysis that takes into account the signalness of the neutrinos, assigning less weight to bronze events. In addition, the updated 90% containment for neutrinos up to 2020 (Abbasi et al. 2023) can be also used for future refined analysis. This approach will enable us to obtain more accurate results.

Our findings increase the total number of TDE or TDE candidates associated with gold neutrinos to five. They all show prominent dust IR echoes and indicate strongly a possible physical connection. The physics of producing high-energy neutrinos in TDEs remains poorly understood. Recently, Winter & Lunardini (2023) developed time-dependent models to interpret the neutrino delays of AT2019dsg, AT2019fdr, and AT2019aalc, assuming that they are the consequence of physical scales of the postdisruption system rather than a statistical effect. They considered three models where neutrinos arise from the interactions of accelerated protons of moderate, medium, and ultra-high energies with X-rays, op-

tical/UV, and IR photons, respectively. In the scenario of dust IR emission serving as the photons, the neutrino delay can be naturally explained by the delayed IR echo at the cost of requiring very high proton energies. In contrast, the optical/UV and X-ray photon scenario cannot describe the observed neutrino time delay as well, while they have higher neutrino production efficiency.

Our work once again highlights the importance of IR time-domain astronomy in studying nuclear transients (see also Jiang et al. 2021a), which may provide insights into the mysterious origin of high-energy neutrinos. It should be noted that our parent sample is constructed from flux-limited SDSS spectroscopic galaxies with a magnitude limit of $r < 17.77$ (Strauss et al. 2002). As a result, we may have missed some TDE counterparts associated with fainter photometric galaxies in our search. For example, the second event AT2019fdr, which was matched with neutrinos and has a redshift of $z = 0.267$, is situated within the SDSS coverage area. However, its faintness ($r = 19.17$) has prevented it from being observed spectroscopically. To address this, we are conducting a more comprehensive blind search for TDE-like IR transients in the known neutrino sky regions using time-resolved WISE images (Z. Y. Zhou et al. in preparation). On the other hand, the persistent optical surveys conducted by ZTF (Yao et al. 2023), along with upcoming more advanced surveys such as the Legacy Survey of Space and Time (LSST; Ivezić et al. 2019) and the Wide-Field Survey Telescope (WFST; Lin et al. 2022; WFST Collaboration et al. 2023), will enable us to build a larger sample of TDEs with IR echoes. This will allow us to arrive at a more con-

clusive conclusion regarding whether or not dusty TDEs are a primary source of high-energy neutrinos. Lastly, it is worth emphasizing that high-energy neutrinos themselves can serve as an independent probe of obscured TDEs, once their connection has been convincingly established.

We sincerely thank the referee for his/her very positive and constructive comments, which help improve our manuscript significantly. We thank useful discussions with Donglian Xu on the declinational dependence of IceCube neutrino detection. This work is supported by SKA Fast Radio Burst and High-Energy Transients Project (2022SKA0130102), the National Natural Science Foundation of China (grants 11833007, 12073025, 12192221), the Fundamental Research Funds for the Central Universities (WK3440000006), and the 111 Project for "Observational and Theoretical Research on Dark Matter and Dark Energy" (B23042). The authors acknowledge the support of Cyrus Chun Ying Tang Foundations. This research uses data obtained through the Telescope Access Program (TAP). Observations obtained with the Hale Telescope at Palomar Observatory were obtained as part of an agreement between the National Astronomical Observatories, Chinese Academy of Sciences, and the California Institute of Technology. We acknowledge the support of the staff of the Lijiang 2.4m telescope. Funding for the telescope has been provided by Chinese Academy of Sciences and the People's Government of Yunnan Province". The ZTF forced-photometry service was funded under the Heising-Simons Foundation grant #12540303 (PI: Graham).

A. APPENDIX

The properties of neutrinos (Table A1) and MIRONG sources used in crossmatch (Table A2).

Table A1. The Information of Neutrinos

ID	Date	Time	Type	R.A.	Decl.	ERRER90	Energy	Signaless
(1)	(2)	(3)	(4)	(5)	(6)	(7)	(8)	(9)
1	22/06/24	16:13:16.40	GOLD	224.1200	41.3100	109.80	192.97	0.60870
2	22/05/13	23:23:12.60	GOLD	224.0300	-1.34000	62.400	207.92	0.56014
3	22/05/09	18:19:04.11	GOLD	334.2500	5.37990	100.79	176.81	0.44648
4	22/04/25	02:44:57.81	GOLD	268.2400	-10.7300	102.59	603.95	0.16877
5	22/04/24	01:06:24.06	GOLD	346.1100	8.91000	68.390	183.99	0.49659
6	22/03/06	03:46:37.06	GOLD	314.8199	8.60990	31.200	413.05	0.77357
7	22/03/03	18:00:07.62	GOLD	267.8000	11.4199	70.790	398.11	0.76419
8	22/02/05	20:08:10.60	GOLD	266.8044	-3.57495	30.800	215.88	0.59235
9	22/02/02	11:48:38.58	GOLD	21.35990	-3.87990	43.790	150.94	0.20564

Table A1 continued

Table A1 (*continued*)

ID	Date	Time	Type	R.A.	Decl.	ERRER90	Energy	Signaless
(1)	(2)	(3)	(4)	(5)	(6)	(7)	(8)	(9)
10	21/11/17	03:50:57.18	GOLD	225.9338	-0.201600	30.800	195.03	0.52590
11	21/09/22	18:17:20.94	GOLD	60.72990	-4.17990	39.000	750.76	0.92534
12	21/08/11	02:02:44.03	GOLD	270.7900	25.2800	56.160	217.67	0.65826
13	21/02/13	18:40:24.51	GOLD	155.2582	-35.3994	71.400	1450.4	0.60730
14	21/02/10	11:53:55.64	GOLD	206.0600	4.78000	52.800	287.41	0.65464
15	20/12/22	00:56:16.14	GOLD	206.3700	13.4399	39.600	185.78	0.53370
16	20/12/21	12:36:53.45	GOLD	261.6899	41.8100	109.20	174.54	0.56429
17	20/12/09	10:15:43.94	GOLD	6.860000	-9.25000	65.400	418.60	0.19226
18	20/11/30	20:21:46.47	GOLD	30.53990	-12.0999	70.790	203.47	0.14696
19	20/11/15	16:01:42.96	GOLD	148.7519	-21.6418	51.890	26182.	0.49261
20	20/11/15	02:07:26.21	GOLD	195.1200	1.37990	77.400	177.38	0.45973
21	20/11/14	15:05:31.96	GOLD	105.2500	6.04990	64.800	214.29	0.56208
22	20/10/07	22:01:49.28	GOLD	265.1700	5.33990	24.000	682.65	0.88552
23	20/09/29	17:48:36.83	GOLD	29.51990	3.47000	31.800	182.89	0.47479
24	20/09/26	07:54:11.62	GOLD	96.45990	-4.33000	39.600	670.50	0.44137
25	20/07/28	08:17:51.99	GOLD	117.5554	-24.8475	30.800	42024.	0.39310
26	20/06/15	14:49:17.37	GOLD	142.9499	3.66000	73.190	496.36	0.82832
27	20/05/30	07:54:29.43	GOLD	255.3700	26.6099	160.19	82.186	0.59170
28	20/01/09	23:41:39.93	GOLD	164.4900	11.8699	174.60	375.23	0.76931
29	19/10/01	20:09:18.17	GOLD	314.0799	12.9399	177.00	217.42	0.58898
30	19/09/22	23:03:55.56	GOLD	5.759900	-1.57000	64.800	187.37	0.50501
31	19/09/22	09:42:45.62	GOLD	167.4300	-22.3900	177.00	3113.9	0.20165
32	19/07/30	20:50:41.31	GOLD	225.7899	10.4700	71.100	298.81	0.67158
33	19/06/19	13:14:18.04	GOLD	343.2599	10.7300	162.59	198.70	0.54551

NOTE— (2)-(3): the Date (yy/mm/dd), and the Time (hh:mm:ss.ss) of the neutrinos. (4): the NoticeType of the neutrino (GOLD or BRONZE). (5)-(6): R.A. and Decl. location of the neutrino (J2000 epoch) in units of degrees. (7): the location uncertainty (radius, 90% containment) in units of arcmin. (8): the Energy most probable neutrino energy that would have produced an event with these observed parameters. (9): the probability this is an astrophysical signal relative to backgrounds.

Table A2. The Information of MIRONG objects

ID	Name	R.A.	Decl.	z	MJD	$\Delta W1$	$\Delta W2$	W1	W2
(1)	(2)	(3)	(4)	(5)	(6)	(7)	(8)	(9)	(10)
1	SDSSJ001249.53+323233.2	3.2064	32.5426	0.1141	59566	0.63	0.93	13.53	12.64
2	SDSSJ002943.36-092233.8	7.4306	-9.3760	0.0736	59551	0.21	0.52	15.69	14.31
3	SDSSJ013455.28-084352.5	23.7303	-8.7312	0.0923	59200	0.40	0.55	14.10	13.03
4	SDSSJ013617.56+282411.3	24.0732	28.4032	0.0707	59420	0.31	0.50	14.76	13.90
5	SDSSJ021640.95-033747.1	34.1706	-3.6298	0.1609	59578	0.90	1.20	14.19	13.29

Table A2 *continued*

Table A2 (*continued*)

ID	Name	R.A.	Decl.	z	MJD	$\Delta W1$	$\Delta W2$	W1	W2
(1)	(2)	(3)	(4)	(5)	(6)	(7)	(8)	(9)	(10)
6	SDSSJ030039.71-082053.8	45.1655	-8.3483	0.0703	58699	0.27	0.53	14.52	13.54
7	SDSSJ035748.65-052239.9	59.4528	-5.3778	0.1127	59081	0.35	0.57	14.38	13.32
8	SDSSJ075544.35+192336.4	118.9348	19.3934	0.1083	59664	0.33	0.52	14.68	13.67
9	SDSSJ081437.37+510141.8	123.6557	51.0283	0.0625	59504	0.81	1.49	13.92	12.75
10	SDSSJ082206.72+273342.6	125.5280	27.5618	0.0965	59147	0.35	0.64	14.40	13.22
11	SDSSJ082358.68+420259.1	125.9945	42.0498	0.1256	59665	0.56	0.85	15.09	14.21
12	SDSSJ082610.41+334457.2	126.5434	33.7492	0.1627	59510	0.93	1.37	14.29	13.26
13	SDSSJ083340.16+324759.5	128.4173	32.7999	0.0513	59669	0.12	0.54	15.89	13.75
14	SDSSJ083653.41+061226.0	129.2225	6.2072	0.1033	58948	0.41	0.64	15.15	14.22
15	SDSSJ084652.32+352741.7	131.7180	35.4616	0.1624	59671	0.34	0.51	14.76	13.81
16	SDSSJ090811.40+262658.7	137.0475	26.4496	0.2076	59313	0.39	0.87	14.58	13.30
17	SDSSJ091308.53+350003.6	138.2856	35.0010	0.1149	58948	0.25	0.62	15.21	13.81
18	SDSSJ091901.51+363536.1	139.7563	36.5934	0.1897	58948	0.30	0.54	14.95	13.71
19	SDSSJ095137.27+341612.4	147.9053	34.2701	0.1322	59687	0.84	1.08	14.31	13.49
20	SDSSJ100809.05+154951.4	152.0377	15.8309	0.1177	59538	0.56	0.88	14.03	12.94
21	SDSSJ100842.62+150409.2	152.1776	15.0692	0.2783	59696	0.86	1.14	14.42	13.43
22	SDSSJ101008.86+300252.6	152.5369	30.0479	0.0874	59691	0.31	0.73	15.70	14.40
23	SDSSJ101107.94+194428.5	152.7830	19.7413	0.0289	59173	0.33	0.79	13.47	12.13
24	SDSSJ101157.62+534857.8	152.9901	53.8161	0.2344	59157	0.46	0.73	14.72	13.50
25	SDSSJ101348.31+180734.9	153.4513	18.1264	0.0120	59696	0.55	0.50	14.02	13.94
26	SDSSJ101708.95+122412.2	154.2873	12.4034	0.1076	59699	0.60	0.98	14.84	13.83
27	SDSSJ102038.51+243708.8	155.1605	24.6191	0.1894	59331	0.85	0.95	13.36	12.58
28	SDSSJ102713.79+150533.2	156.8074	15.0925	0.1839	59178	1.24	1.32	13.75	13.03
29	SDSSJ104832.79+122857.2	162.1366	12.4825	0.0537	58977	0.59	1.11	13.65	12.60
30	SDSSJ110138.83+285039.2	165.4119	28.8442	0.0344	59338	0.37	0.54	14.27	13.55
31	SDSSJ111156.67+361707.3	167.9861	36.2854	0.0786	58970	0.34	0.68	14.44	13.18
32	SDSSJ111431.84+405613.8	168.6327	40.9372	0.1525	58968	0.53	0.60	14.02	13.11
33	SDSSJ111614.66+061736.2	169.0611	6.2934	0.0754	59194	0.71	1.04	13.61	12.80
34	SDSSJ112108.22+505219.6	170.2842	50.8721	0.1513	59330	0.51	0.74	14.82	13.54
35	SDSSJ112526.86+070520.3	171.3619	7.0890	0.0957	58828	0.32	0.59	15.10	14.03
36	SDSSJ112858.33+210257.5	172.2431	21.0493	0.1619	59555	0.42	0.60	15.08	14.25
37	SDSSJ112939.08+365301.2	172.4128	36.8837	0.1995	59182	0.83	1.10	15.10	14.18
38	SDSSJ115205.33+485050.0	178.0222	48.8472	0.1510	59179	0.96	1.21	13.66	12.73
39	SDSSJ115812.34+384332.3	179.5514	38.7257	0.0742	59344	0.25	0.75	15.72	14.07
40	SDSSJ120344.13+543331.7	180.9339	54.5588	0.1052	59334	0.51	0.85	14.86	13.94
41	SDSSJ120444.71+104642.3	181.1863	10.7784	0.0685	59566	0.75	1.19	12.55	11.26
42	SDSSJ120813.78+513504.2	182.0574	51.5845	0.0889	59179	0.21	0.75	15.89	14.06
43	SDSSJ121249.92+024012.9	183.2080	2.6703	0.0772	59571	0.22	0.63	16.33	14.89
44	SDSSJ121337.51+051730.8	183.4063	5.2919	0.1398	58842	0.24	0.52	15.79	14.66
45	SDSSJ121738.27+035040.5	184.4094	3.8447	0.0731	59207	0.37	0.75	14.37	13.31

Table A2 *continued*

Table A2 (*continued*)

ID	Name	R.A.	Decl.	z	MJD	$\Delta W1$	$\Delta W2$	W1	W2
(1)	(2)	(3)	(4)	(5)	(6)	(7)	(8)	(9)	(10)
46	SDSSJ121825.52+295154.8	184.6063	29.8652	0.1356	59197	0.89	1.57	14.23	12.82
47	SDSSJ123155.15+323240.4	187.9798	32.5445	0.0654	59721	1.14	1.44	12.20	11.42
48	SDSSJ123431.24+235338.4	188.6302	23.8942	0.2787	58995	0.45	0.61	14.90	14.06
49	SDSSJ124754.96-033738.7	191.9790	-3.6274	0.0903	59216	1.14	1.48	11.78	10.87
50	SDSSJ125953.97+060050.3	194.9749	6.0140	0.1060	59011	0.41	0.65	14.61	13.61
51	SDSSJ130617.74+533907.1	196.5739	53.6520	0.0300	59555	0.40	0.74	13.23	12.23
52	SDSSJ132338.83+275420.2	200.9118	27.9056	0.0730	58847	0.55	1.43	13.88	12.12
53	SDSSJ134148.78+370047.2	205.4533	37.0131	0.1968	59006	0.50	0.73	14.68	13.68
54	SDSSJ134419.60+512624.8	206.0816	51.4402	0.0629	59199	0.58	0.77	12.69	11.90
55	SDSSJ134821.40+024914.9	207.0892	2.8208	0.0855	59593	0.77	1.29	13.53	12.49
56	SDSSJ134958.72-001120.9	207.4947	-0.1891	0.1020	59595	0.32	0.55	15.18	14.20
57	SDSSJ135246.87+202444.0	208.1953	20.4122	0.0544	59223	0.66	1.19	13.88	12.86
58	SDSSJ135251.12+161317.2	208.2130	16.2214	0.1578	58858	0.51	0.82	14.79	13.76
59	SDSSJ140515.60+542458.1	211.3150	54.4161	0.0833	59359	0.45	0.71	14.84	13.99
60	SDSSJ141249.70+151254.7	213.2071	15.2152	0.1411	59594	1.01	1.33	13.96	13.18
61	SDSSJ141437.38-002800.8	213.6557	-0.4669	0.2611	59236	0.18	0.56	16.67	14.70
62	SDSSJ142237.73+284424.3	215.6572	28.7401	0.1250	59384	0.64	1.17	14.26	13.01
63	SDSSJ142420.79+624916.4	216.0866	62.8212	0.1091	59713	0.39	0.62	14.32	13.40
64	SDSSJ142727.72+162347.5	216.8655	16.3965	0.1278	59233	1.05	1.50	14.01	13.26
65	SDSSJ142813.88+391218.6	217.0578	39.2052	0.2583	58651	0.60	0.62	14.08	13.37
66	SDSSJ143016.05+230344.4	217.5668	23.0623	0.0810	58866	0.68	0.93	12.62	11.78
67	SDSSJ143114.72+171135.4	217.8113	17.1932	0.0378	58869	0.81	1.22	15.23	14.24
68	SDSSJ143701.26+073508.4	219.2553	7.5857	0.1830	59238	0.84	1.15	13.69	12.53
69	SDSSJ143701.72+532358.4	219.2572	53.3996	0.0469	59208	0.42	0.75	13.85	13.01
70	SDSSJ144227.60+555846.4	220.6150	55.9796	0.0769	59205	1.36	1.83	11.67	10.81
71	SDSSJ145501.50+084427.8	223.7562	8.7411	0.1601	58878	0.29	0.73	15.62	13.94
72	SDSSJ150440.39+010735.0	226.1683	1.1264	0.1283	59613	0.67	0.75	12.37	11.35
73	SDSSJ151828.07+191636.6	229.6170	19.2768	0.0894	59244	0.28	0.55	15.43	14.42
74	SDSSJ152223.27+014626.1	230.5970	1.7739	0.0785	59253	0.41	0.61	14.38	13.67
75	SDSSJ152535.07+082157.5	231.3961	8.3660	0.0754	59616	0.42	0.99	15.73	14.35
76	SDSSJ153239.62+443203.1	233.1651	44.5342	0.0376	59234	1.00	1.76	13.54	12.40
77	SDSSJ154357.60+100613.5	235.9900	10.1037	0.1753	59256	0.92	1.42	14.37	13.33
78	SDSSJ154843.07+220812.7	237.1795	22.1369	0.0313	59253	2.56	3.48	11.18	10.16
79	SDSSJ154849.49+125513.9	237.2062	12.9205	0.1433	59418	0.53	0.93	14.97	13.71
80	SDSSJ155259.95+210246.9	238.2498	21.0463	0.1717	59417	0.96	1.24	14.69	13.75
81	SDSSJ155440.26+362952.0	238.6678	36.4978	0.2368	59246	0.88	1.21	14.23	13.26
82	SDSSJ155633.99+174200.8	239.1416	17.7002	0.1359	59419	0.43	0.62	15.22	14.31
83	SDSSJ160014.59+180400.0	240.0608	18.0667	0.1381	59053	0.27	0.51	15.49	14.35
84	SDSSJ161258.17+141617.6	243.2424	14.2715	0.0720	59262	0.43	0.88	14.75	13.34
85	SDSSJ164938.77+262515.3	252.4116	26.4211	0.0588	59068	1.41	2.29	13.09	11.92

Table A2 *continued*

Table A2 (*continued*)

ID	Name	R.A.	Decl.	z	MJD	$\Delta W1$	$\Delta W2$	W1	W2
(1)	(2)	(3)	(4)	(5)	(6)	(7)	(8)	(9)	(10)
86	SDSSJ165516.63+382802.5	253.8193	38.4674	0.1005	58699	0.39	0.65	15.36	14.43
87	SDSSJ170503.58+344010.3	256.2649	34.6695	0.1659	58706	0.18	0.58	16.55	14.89
88	SDSSJ214906.34+122519.6	327.2764	12.4221	0.0596	58791	0.28	0.59	14.98	13.53
89	SDSSJ215055.73-010654.2	327.7322	-1.1151	0.0879	58990	1.79	1.96	13.83	12.94
90	SDSSJ221541.60-010721.1	333.9233	-1.1225	0.0478	58996	0.24	0.68	14.17	12.75
91	SDSSJ223628.13+142830.9	339.1172	14.4753	0.2649	59738	0.25	0.58	15.97	14.63
92	SDSSJ225549.89+001728.5	343.9579	0.2913	0.1111	59372	0.29	0.89	15.87	14.14
93	SDSSJ233517.46+010421.1	353.8227	1.0725	0.0806	59745	0.42	0.78	14.91	13.89
94	SDSSJ235911.19+011006.8	359.7966	1.1686	0.0985	58655	0.79	0.96	13.71	12.98

NOTE— (1): the ID of MIRONG sources with W2 peak time in the same range of neutrinos listed in Appendix Table A1, that is between June 2019 June and June 2022. (2)-(5): the Name, R.A., Decl. and redshift of these objects. (6): the Modified Julian Date (MJD) of the W2 peak. (7)-(8): the variability amplitudes in W1 and W2 band, respectively. (9)-(10): the W1 and W2 magnitudes with flux of quiescent state subtracted.

REFERENCES

- Aartsen, M. G., Ackermann, M., Adams, J., et al. 2020, *PhRvL*, 124, 051103
- Abbasi, R., Ackermann, M., Adams, J., et al. 2023, arXiv:2304.01174
- Baldwin, J. A., Phillips, M. M., & Terlevich, R. 1981, *PASP*, 93, 5
- Cendes, Y., Alexander, K. D., Berger, E., et al. 2021, *ApJ*, 919, 127
- Fan, Y.-F., Bai, J.-M., Zhang, J.-J., et al. 2015, *Research in Astronomy and Astrophysics*, 15, 918
- Frederick, S., Gezari, S., Graham, M. J., et al. 2021, *ApJ*, 920, 56
- Gezari, S. 2021, *ARA&A*, 59
- Hammerstein, E., van Velzen, S., Gezari, S., et al. 2023, *ApJ*, 942, 9
- Graham, M. J., Djorgovski, S. G., Drake, A. J., et al. 2017, *MNRAS*, 470, 4112
- IceCube Collaboration 2013, *Science*, 342, 1242856
- IceCube Collaboration, Aartsen, M. G., Ackermann, M., et al. 2018, *Science*, 361, 147.
- IceCube Collaboration, Abbasi, R., Ackermann, M., et al. 2022, *Science*, 378, 538
- Ivezić, Ž., Kahn, S. M., Tyson, J. A., et al. 2019, *ApJ*, 873, 111
- Jiang, N., Dou, L., Wang, T., et al. 2016, *ApJL*, 828, L14
- Jiang, N., Wang, T., Mou, G., et al. 2019, *ApJ*, 871, 15
- Jiang, N., Wang, T., Dou, L., et al. 2021a, *ApJS*, 252, 32
- Jiang, N., Wang, T., Hu, X., et al. 2021b, *ApJ*, 911, 31
- Kool, E. C., Reynolds, T. M., Mattila, S., et al. 2020, *MNRAS*, 498, 2167
- Liao, N.-H., Sheng, Z.-F., Jiang, N., et al. 2022, *ApJL*, 932, L25
- Lin, Z., Jiang, N., & Kong, X. 2022, *MNRAS*, 513, 2422
- Mainzer, A., Bauer, J., Cutri, R. M., et al. 2014, *ApJ*, 792, 30
- Masci, F. J., Laher, R. R., Rusholme, B., et al. 2019, *PASP*, 131, 018003
- Mattila, S., Pérez-Torres, M., Efstathiou, A., et al. 2018, *Science*, 361, 482
- Nicholl, M., Blanchard, P. K., Berger, E., et al. 2020, *Nature Astronomy*, 4, 893
- Oke, J. B. & Gunn, J. E. 1982, *PASP*, 94, 586
- Panagiotou, C., De, K., Masterson, M., et al. 2023, *ApJL*, 948, L5
- Pitík, T., Tamborra, I., Angus, C. R., et al. 2022, *ApJ*, 929, 163
- Rees, M. J. 1988, *Nature*, 333, 523
- Reusch, S., Stein, R., Kowalski, M., et al. 2022, *PhRvL*, 128, 221101
- Stein, R., van Velzen, S., Kowalski, M., et al. 2021, *Nature Astronomy*, 5, 510
- Strauss, M. A., Weinberg, D. H., Lupton, R. H., et al. 2002, *AJ*, 124, 1810
- Trakhtenbrot, B., Arcavi, I., Ricci, C., et al. 2019, *Nature Astronomy*, 3, 242
- van Velzen, S., Mendez, A. J., Krolik, J. H., & Gorjian, V. 2016, *ApJ*, 829, 19
- van Velzen, S., Gezari, S., Hammerstein, E., et al. 2021, *ApJ*, 908, 4
- van Velzen, S., Stein, R., Gilfanov, M., et al. 2021, arXiv:2111.09391
- van Velzen, S., Pasham, D. R., Komossa, S., et al. 2021, *SSRv*, 217, 63

- Wang, C.-J., Bai, J.-M., Fan, Y.-F., et al. 2019, *Research in Astronomy and Astrophysics*, 19, 149
- Wang, Y., Jiang, N., Wang, T., et al. 2022a, *ApJS*, 258, 21
- Wang, Y., Jiang, N., Wang, T., et al. 2022b, *ApJL*, 930, L4
- WFST Collaboration, Wang, T., Liu, G., et al. 2023, [arXiv:2306.07590](https://arxiv.org/abs/2306.07590)
- Winter, W. & Lunardini, C. 2023, *ApJ*, 948, 42
- Wright, E. L., Eisenhardt, P. R. M., Mainzer, A. K., et al. 2010, *AJ*, 140, 1868-1881
- Yao, Y., Ravi, V., Gezari, S., et al. 2023, [arXiv:2303.06523](https://arxiv.org/abs/2303.06523)